MATHEMATICAL BIOSCIENCES
AND ENGINEERING
Volume **1**, Number **2**, September **2004**

http://math.asu.edu/~mbe/

pp. **339–346**

SYNCHRONIZATION BETWEEN TWO HELE-SHAW CELLS

A. Bernardini, J. Bragard, and H. Mancini

Department of Physics and Applied Mathematics
University of Navarra
Irunlarrea, s/n
31080 Pamplona, Spain

(Communicated by Stefano Boccaletti)

Abstract. Complete synchronization between two Hele-Shaw cells is examined. The two dynamical systems are chaotic in time and spatially extended in two dimensions. It is shown that a large number of connectors are needed to achieve synchronization. In particular, we have studied how the number of connectors influences the dynamical regime that is set inside the Hele-Shaw cells.

1. **Introduction.** Synchronization phenomena are abundant in science, nature, engineering, and social life. Systems as diverse as clocks, singing crickets, cardiac pacemakers, and applauding audiences exhibit a tendency to operate in synchrony [1, 2]. In the last few years, synchronization of chaotic dynamics [3, 4, 5] has gained much interest in view of its applications in communications systems [6, 7]. Different coupling schemes have been proposed to achieve synchronization [3, 7, 8]. A widely used coupling-, and controlling-, technique is the so-called pinning technique [9, 10] which connects pair of points in the two systems. Recently, the effect of asymmetries in the coupling [11] has been demonstrated to be a key parameter in the synchronization of spatially extended systems.

In this paper, we analyze possible synchronization mechanisms between two Hele-Shaw cells. The Hele-Shaw cell has been extensively investigated in the context of porous-media convection, since it has a clear geophysical interest [12, 13, 14, 15]. A Hele-Shaw cell is a rectangular cavity where the gap between two vertical walls is much smaller than the other two spatial dimensions. For this reason, the governing equations for gap-averaged velocity components are identical with those for two-dimensional flow in a porous medium [16, 17]. Thermal convection inside a porous medium can be studied and easily visualized in the laboratory with the help of a Hele-Shaw cell.

The Rayleigh number is the parameter that indicates the temperature difference between the bottom and the top of the container. In a porous medium, when the Rayleigh number is increased above a critical threshold value of $Ra_c = 4\pi^2$, the heat transfer changes from conduction to convection. This first transition has already received considerable attention by Horton and Rogers [18] and Lapwood [15]. Further increasing the Rayleigh number causes the flow to become oscillatory. The appearance of time-dependent motion in a fluid layer uniformly heated from

2000 *Mathematics Subject Classification.* 76R10,76F70,76F45.
Key words and phrases. Complete synchronization, Hele-Shaw cell, convection.

below has been suggested from Caltagirone et al. [19] who verified experimentally the existence of stationary and oscillatory motions. In this paper the dynamical regimes ranging from $Ra = 44$ to $Ra = 1200$ have been computationally studied. Our simulations have confirmed the old numerical and experimental results. In studying the synchronization between two convective Hele-Shaw cells, the main objective is to examine the interaction of the boundary-layer instability occurring in two connected cells.

The governing equations are introduced in the next section. Section 3 is dedicated to explaining the numerical procedure. In section 4, we illustrate the different dynamical regimes as a function of the Rayleigh numbers. In the last section we present some attempts at synchronizing two Hele-Shaw cells in the chaotic regime, and we show that *(i)* synchronization may be achieved by connecting all the internal points of the two systems; *(ii)* connection through the lateral walls only is insufficient to synchronize the cells and *(iii)* with a reduced number of internal connectors, synchronization may still be achieved, but the dynamical regime is strongly perturbed.

2. **The governing equations.** The dynamical system modelled here consists of two Hele-Shaw cells that are thermally connected. Let us recall the equations that govern a single Hele-Shaw cell. A bounded two-dimensional square porous layer of thickness h is considered. The vertical boundaries are adiabatic and the horizontal boundaries are isothermal. The temperature difference across the porous layer is fixed to ΔT; the porous layer is heated from below. The porous medium has a porosity ϕ, an isotropic permeability k, a heat capacity $(\rho c)_s$ (subscript s designates the solid matrix), and it is saturated with an incompressible fluid that has a constant dynamic viscosity μ, a coefficient of thermal expansion α, a density ρ, and a heat capacity $(\rho c)_f$ (subscript f designates the fluid properties). The thermal conductivity of the fluid-saturated porous medium is λ. We use the Boussinesq approximation and assume that the flow velocity obeys Darcy's law (the inertial terms are neglected). Under these assumptions, the equations governing the flow within the porous medium are

$$\phi \frac{\partial \rho_f}{\partial t} + \nabla \cdot (\rho_f \mathbf{v}) = 0, \tag{1}$$

$$\mathbf{v} = \frac{k}{\mu}(-\nabla p + \rho_f \mathbf{g}), \tag{2}$$

$$(\phi(\rho c)_f + (1-\phi)(\rho c)_s) \frac{\partial T}{\partial t} + (\rho c)_f \mathbf{v} \cdot \nabla T = \lambda \nabla^2 T, \tag{3}$$

$$\rho_f = \rho_0[1 - \alpha(T - T_0)], \tag{4}$$

where $\mathbf{g}$ is the acceleration due to gravity. Since ϕ is small for most relevant systems, the energy equation can be reduced to

$$\sigma \frac{\partial T}{\partial t} + \mathbf{v} \cdot \nabla T = \kappa \nabla^2 T, \tag{5}$$

where $\sigma = (\rho c)_s/(\rho c)_f$ is typically close to unity and κ is the thermal diffusivity of the fluid-saturated porous medium. The explicit appearance of the pressure gradient can be avoided by using the stream-function reformulation. The problem is written in dimensionless form by scaling lengths with h, time with h^2/κ, temperature with ΔT, and the velocity with κ/h. Keeping the same notation for all the

dimensionless variables and assuming that $\sigma = 1$, the dimensionless equations are

$$\frac{\partial T}{\partial t} = \nabla^2 T - \frac{\partial \psi}{\partial y}\frac{\partial T}{\partial x} + \frac{\partial \psi}{\partial x}\frac{\partial T}{\partial y}, \tag{6}$$

$$\nabla^2 \psi = -Ra\frac{\partial T}{\partial x}, \tag{7}$$

where Ra is the Rayleigh number and is defined by

$$Ra = \frac{\alpha g k \rho_0 h \Delta T}{\mu \kappa}. \tag{8}$$

This number is a dimensionless parameter that measures the applied temperature difference. The Jacobian non linear term in (6) comes from the advection term in the energy equation; we shall denote it by J from now on. The boundary conditions are

$$T(x,0) = 1, \qquad T(x,1) = 0, \tag{9}$$

and for the adiabatic conditions at the lateral walls:

$$\frac{\partial T}{\partial x}(0,y) = \frac{\partial T}{\partial x}(1,y) = 0. \tag{10}$$

The stream function vanishes at all boundaries because of the impermeability of the walls.

3. **Computational techniques.** In this section, we give a brief outline of the numerical scheme used to solve Equations (6) and (7). The finite-difference scheme has already been proposed in [12, 13] and for a related problem in [14]. The main drawback of the use of a finite-difference scheme in the stream-function formulation is that it may lead to numerical instability. Indeed, a center discretization for the advection term (J) causes numerical instability due to the occurrence of aliasing errors. To avoid this numerical instability, we discretize the advection term using a second-order Arakawa term [12].

Let us recall how the scheme is implemented. Space derivatives are discretized by using second-order centered differences at the internal grid point (i,j) for $i = 1, ..., N-1$ and $j = 1, ..., M-1$ ($i = 0$ or N or $j = 0$ or M represent the points at the boundary). Special treatment is used for the advection term (Arakawa discretization) [12]. In Equation (6), time is advanced explicitly by using a second-order Adams-Bashforth formula:

$$\frac{T^* - T^n}{\Delta t} = \frac{3}{2}J(T^n, \psi^n) - \frac{1}{2}J(T^{n-1}, \psi^{n-1}), \tag{11}$$

where the superscripts represent the actual time step. The asterisk denotes an intermediate step that is necessary in the implicit calculation for the Laplacian term by an alternating-implicit direction method [20] . The time step is completed with

$$\frac{T^{n+1} - T^*}{\Delta t} = \nabla^2\left(\frac{T^{n+1} - T^*}{2}\right). \tag{12}$$

Dirichlet boundary conditions are applied setting $T_{0j} = 1$, $T_{Nj} = 0$, and $\psi_{ij} = 0$. Second-order accurate Neumann boundary conditions are applied using three-points formula:

$$T_{i,0} = \frac{4T_{i,1} - T_{i,2}}{3}, \qquad T_{i,N} = \frac{4T_{i,N-1} - T_{i,N-2}}{3}. \tag{13}$$

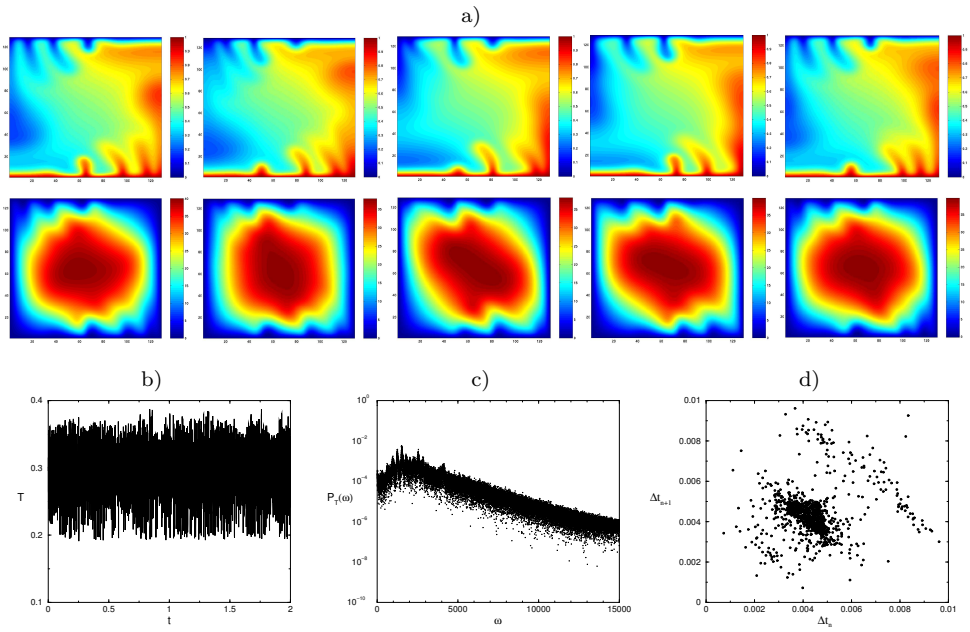

FIGURE 1. (a) Snapshots of temperature and stream function for the solution at $Ra = 1200$ taken at regular time interval ($\Delta\tau = 10^{-3}$). (b) Time evolution of the temperature taken at point $(x, y) = (1/3, 1/3)$. (c) The power spectrum of the signal shown in (b) in a log-linear scale illustrates the region of exponential decay in the high frequency domain. (d) The Poincaré section of the signal shown in (b) clearly indicates a chaotic regime.

The Poisson equation is efficiently solved by the generalized cyclic reduction routine BLKTRI from the FISHPACK package [21]. Simulations are performed, for $Ra = 1200$, with a time step $\Delta t = 10^{-5}$ and a mesh grid with 129×129 points.

4. **Numerical results.** In this section, the results of some numerical simulations for a single Hele-Shaw cell are presented. By increasing the control parameter (Rayleigh number), we observe a succession of different dynamical regimes. At low Rayleigh number, $Ra = 44$, the conductive solution becomes unstable and a convective flow sets in. The flow is steady and organizes itself following the most unstable mode; that is, the uni-cellular mode. The single-roll solution can turn clockwise or counterclockwise depending on the initial condition. The uni-cellular convection mode dominates for the low Rayleigh number regimes until $Ra = 350$. For intermediate Rayleigh number regime, the uni-cellular convection mode competes with multi-cellular steady convective pattern. Again, the selection of the solution depends crucially on the initial condition [19]. At $Ra = 400$, the uni-cellular mode becomes oscillating. The convection is no longer periodic at $Ra = 500$, where there is a new second fundamental frequency, incommensurable with the first. For this Rayleigh number, we observe for the first time the formation of thermal plumes. As an operational definition, a plume is formed when an isotherm in the boundary layer is buckled. At $Ra = 570$, the uni-cellular mode returns to a simply periodic regime. At $Ra = 1100$, the cell goes back to a quasi-periodic regime. At $Ra = 1200$, the uni-cellular mode is chaotic, and a strong broad-band

noise appears in the power spectrum, as shown in Figure 1c. Exponential decay in the power spectra at high frequency is expected for bounded smooth deterministic dynamics [22, 23]. The Poincaré section shows a large number of scattered points. Qualitatively, however, the flow pattern appears to follow a cycle, characterized by the boundary-layer instability and the release of thermal plumes without any specific regularity.

5. **Synchronization.** The aim of the present investigation is the study of synchronization between two Hele-Shaw cells in the space-time chaotic regime (hereinafter fixed to $Ra = 1200$). In particular, we are considering different ways of connecting the two cells and what is the resulting synchronized state.

5.1. **All internal points are connectors.** Starting from two identical Hele-Shaw cells, prepared with counterclockwise flow rotation but different initial conditions, we set a thermal bidirectional coupling between *all* the internal points. Adding the dissipation term to Equations (6) and (7), the dynamics of the cells is now governed by

$$I \quad \begin{cases} \dfrac{\partial T^{(1)}}{\partial t} &= \nabla^2 T^{(1)} + J(T^{(1)}, \psi^{(1)}) + \epsilon(T^{(2)} - T^{(1)}) \\ \nabla^2 \psi^{(1)} &= -Ra \dfrac{\partial T^{(1)}}{\partial x} \end{cases} \tag{14}$$

$$II \quad \begin{cases} \dfrac{\partial T^{(2)}}{\partial t} &= \nabla^2 T^{(2)} + J(T^{(2)}, \psi^{(2)}) + \epsilon(T^{(1)} - T^{(2)}) \\ \nabla^2 \psi^{(2)} &= -Ra \dfrac{\partial T^{(2)}}{\partial x}\,, \end{cases} \tag{15}$$

where the indexes 1 and 2 refer to the two cells, and ϵ is the thermal coupling and is applied in all the internal points ($i, j = 1, ..., N-1$). For several coupling strengths, $\epsilon = 0.5; 0.05; 0.02; 0.01$, set at the dimensionless time $t = 0.01$, the synchronization error is defined by

$$E = \sum_r |T^{(1)}(r) - T^{(2)}(r)|, \tag{16}$$

where r stands for all the interior points, is monitored vs. time (see Figure 2). As expected, the rate of convergence to the synchronized state is faster for stronger couplings. One observes that there is a critical value of the coupling below which synchronization is no longer obtained.

5.2. **Coupling only through the lateral walls.** We have shown theoretically that synchronization between two Hele-Shaw cells is possible for sufficiently large coupling strengths. The next question that we want to address here is related to the experimental realization of this synchronization. Indeed, connecting two space-extended systems is certainly no easy task. An obvious limitation is how practically to implement the coupling between the two convective cells without totally destroying the dynamics. The coupling technique used thus far involved connecting the whole spatial domain of the two cells. It is still unclear how to realize such a connection between all the internal points of the cells. This may also be impractical in experiments. Figure 3 displays the horizontal spatial correlation function at different heights. Because of the small spatial correlation length [24] (see Figure 3), it seems (at least intuitively) that we will need to put several internal connectors

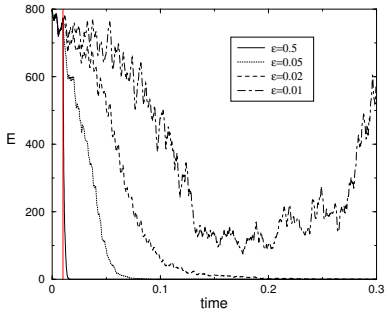

FIGURE 2. Synchronization error E (see text for definition) vs. time, for several values of the coupling strength (ϵ). For $\epsilon = 0.01$, synchronization is not achieved.

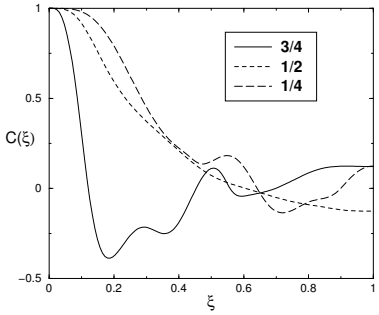

FIGURE 3. The spatial correlation function of the temperature for $x \in [0, 1]$, at $y = 1/4$, $y = 1/2$, and $y = 3/4$.

between the two cells to achieve synchronization. This number of connectors must be finite and, ideally, as small as possible. In addition, one should mention that experimental measuring devices have a finite space and time resolution, which also is a practical limit in the number of independent connectors.

To test the feasibility of an experiment with a reduced number of connectors, we put connectors only at the lateral walls; that is, 256 mesh points for each cell. With this particular choice the system is still governed by equations (14 and 15), but the term $\epsilon(T^{2,1}_{i,j} - T^{1,2}_{i,j})$ is different from zero for $i = 1, ..., N-1$, only at $j = 1$ and $j = N-1$. The synchronization errors (not shown here) suggest that this type of connection is not strong enough to achieve synchronization.

5.3. **Finite number of internal points are used as connectors.** We have shown that the synchronization of the two cells cannot be achieved by only connecting through the lateral walls. An intermediate situation is considered now. Let us investigate the minimal number of "internal" points needed to obtain synchronization. In an experiment, one will always try to use as few controllers as possible. The simplest way to start investigating the minimal number of controllers is to put the connectors every two grid points and, in case of success, following the reduction of connectors in this way. For a connector every two grid points, one observes synchronization (see Figure 4), but the flow passes from a single-roll cell (chaotic) to a three-cellular convection mode (stationary). The convergence to the synchronized state is rather slow compared to the case of all point connectors. One observes that the final dynamical state of the system (chaos suppression in this

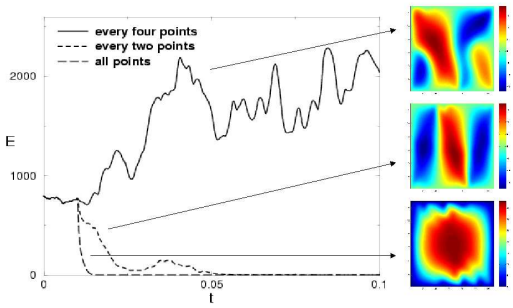

FIGURE 4. The synchronization error obtained by connecting all, every two, and every four internal points. The coupling parameter ($\epsilon = 0.5$) is set at $t = 0.01$. For a loose connection (every two points) a new three-cellular stationary structure appears in both cells. For a connector every four points, synchronization is not achieved.

case) is highly dependent on the number of connectors. An explanation for this fact is that the basin of attraction of the single chaotic cell is quite narrow, and a sparse and strong coupling lead to fall in the three-cellular steady solution. In the case of a connector every four grid points, which corresponds to a reduction by a factor 16 of the number of connectors, synchronization is no longer achieved. The solution with a single chaotic cell is destroyed and is replaced by a two-cellular chaotic solution (see Figure 4).

6. **Conclusions.** The number of connectors needed to synchronize two Hele-Shaw cells in the chaotic regime ($Ra = 1200$) has been studied. We have proven that this fluid system is particularly difficult to synchronize. Our study provides a numerical benchmark for further investigation in the direction of control and synchronization of unstable boundary layers. The practical relevance in fluid mechanics systems is currently investigated [25] by many research laboratories.

Acknowledgments. A. Bernardini is supported by the European project COSYC of SENS (grant Number HPRN-CT-2000-00158). Financial support from MCYT project (Spain) BFM2002-02011 (INEFLUID) is also acknowledged.

REFERENCES

[1] A. Pikovsky, M. Rosenblum, and J. Kurths, "Synchronization, A Universal Concept in Nonlinear Sciences," Cambridge University Press, UK, 2001.
[2] S. Boccaletti, J. Kurths, G. Osipov, D.L. Valladares, and C.S. Zhou, THE SYNCHRONIZATION OF CHAOTIC SYSTEMS, Phys. Rep., 366 (2002), 1–101.
[3] L.M. Pecora and T.L. Carroll, SYNCHRONIZATION IN CHAOTIC SYSTEMS, Phys. Rev. Lett., 64 (1990), 821–824.
[4] V.S. Anishchenko, T.E. Vadivasova, D.E. Postnoy, and M.A. Safonova, SYNCHRONIZATION OF CHAOS, Int. J. Bifurc. Chaos, 2 (1992), 633–644.
[5] R. Femat and G. Solis–Perales, ON THE CHAOS SYNCHRONIZATION PHENOMENA, Phys. Letts. A, 262 (1999), 50–60.
[6] L. Kocarev and U. Parlitz, GENERAL APPROACH FOR CHAOTIC SYNCHRONIZATION WITH APPLICATIONS TO COMMUNICATION, Phys. Rev. Lett., 74 (1995), 5028–5031.
[7] U. Parlitz, L. Kocarev, T. Stojanovski, and H. Preckel, ENCODING MESSAGES USING CHAOTIC SYNCHRONIZATION, Phys. Rev. E, 53 (1993), 4351–4361.

[8] L. Junge and U. Parlitz, Synchronization and control of coupled Ginzburg-Landau equations using local coupling, Phys. Rev. E, 61 (2000), 3736–3742.
[9] G. Hu and Z. Qu, Controlling spatiotemporal chaos in coupled map lattice systems, Phys. Rev. Lett., 72 (1994), 68–71.
[10] R.O. Grigoriev, M.C. Cross, and H.G. Schuster, Pinning control of spatiotemporal chaos, Phys. Rev. Lett., 79 (1997), 2795–2798.
[11] J. Bragard, S. Boccaletti, and H. Mancini, Asymmetric coupling effects in the Synchronization of spatially extended chaotic systems, Phys. Rev. Lett., 91 (2003), 064103.
[12] R.N. Horne and M.J. O'Sullivan, Oscillatory convection in a porous medium heated from below, J. Fluid Mech., 66, 1974, 339–352.
[13] M.D. Graham and P.H. Steen, Plume formation and resonant bifurcations in porous-media convection, J. Fluid Mech., 272 (1994), 67–89.
[14] A.S.M. Cherkaoui and W.S.D. Wilcock, Characteristics of high Rayleigh number two-dimensional convection in an open-top porous layer heated from below, J. Fluid Mech., 394 (1999), 241–260.
[15] E.R. Lapwood, Convection of a fluid in a porous medium, Proc. Camb. Phil. Soc., 44 (1948), 508–521.
[16] J. Bear, "Dynamics of Fluid in Porous Media," Dover, New York, 1972.
[17] D.A. Nield and A. Bejan, "Convection in Porous Media," Springer, New York, 1999.
[18] C.W. Horton and F.T. Rogers, J. Appl. Phys. , 16 (1945), 367.
[19] J.P. Caltagirone, M. Cloupeau, and M. Combarnous, Convection naturelle fluctuante dans une couche poreuse horizontale, Acad. Sci. Paris, 273 (1971), 833–836.
[20] W.H. Press, "Numerical Recipes in FORTRAN: The Art of Scientific Computing," Cambridge University Press, Cambridge, 1992.
[21] P.N. Swarzttrauber and R.A. Sweet, Efficient FORTRAN subprograms for the solution of elliptic partial differential equations, ACM Trans. Math. Soft., 5 (1979), 352.
[22] M.R. Paul, M.C. Cross, P.F. Fischer, and H.S. Greenside, Power law behavior of power spectra in low Prandtl number Rayleigh Bénard convection, Phys. Rev. Lett., 87 (2001), 154501/1–4.
[23] U. Frisch and R. Morf, Intermittency in nonlinear dynamics and singularities at complex times, Phys. Rev. A, 23 (1981), 2673–2705.
[24] P. Bergé, Y. Pomeau, and Ch. Vidal, "L'ordre dans le chaos," Hermann, Paris, 1984.
[25] L. Cortelezzi and J.L. Speyer, Robust Reduced-Order Controller of Laminar Boundary Layer Transitions, Phys. Rev. E, 58 (1998), 1906–1910.

Received on Feb. 1, 2004. Revised on May 4, 2004.

E-mail address: angela@fisica.unav.es
E-mail address: jbragard@fisica.unav.es
E-mail address: hmancini@fisica.unav.es